ICAS-98-3,3,1. (21st Congress of the International Council of the Aeronautical Sciences) Sept. 1998, Melbourne, Australia

LUMINESCENT PAINT TECHNOLOGY FOR TEMPERATURE AND PRESSURE MEASUREMENTS IN A CRYOGENIC WIND TUNNEL

Keisuke Asai*
Aerodynamics Division
National Aerospace Laboratory
Tokyo, JAPAN

John P. Sullivan†
School of Aeronautics and Astronautics
Purdue University
West Lafayette, Indiana, USA

ABSTRACT

In recent experiments, we demonstrated the feasibility of using luminescent paints for temperature and pressure measurements in a cryogenic wind tunnel. This technique is based on the photo-physical processes known as thermal- and oxygen-quenching. Through these processes, the luminescent intensity of the paint emission can be related to temperature or pressure. Verification tests have been performed in NAL 0.1-m Transonic Cryogenic Wind Tunnel. Using temperature-sensitive paints based on ruthenium complex and silicone polymer, boundary-layer transition on an airfoil model has been successfully detected from 90 to 150 Kelvin. Likewise, using pressure-sensitive coating based on ruthenium molecules and anodized porous alumina, surface pressure field including shock waves and flow separation has been clearly captured in cryogenic flow. As has been demonstrated by these experiments, the luminescent paint technology works in the adverse flow condition in a cryogenic wind tunnel. It would be possible to develop the cryogenic TSP and PSP systems that is much superior to that for ambient-temperature testing.

NOMENCLATURE

A, B	= calibration coefficients of paint
c	= chord length, m
Cp	= pressure coefficient, $(p-p_\infty)/q_\infty$
I	= intensity, counts
Kq	= Stern-Volmer coefficient with respect to [O2]
k	= rate constant, 1/sec
M	= Mach number
p	= pressure, kPa
q	= dynamic pressure, kPa
r	= recovery factor
Re	= Reynolds number
T	= temperature, K
x	= chordwise location, m
$\overline{X}_{o2}$	= mole fraction of oxygen in flow, % or ppm
α	= angle of attack, degree
Φ	= quantum efficiency

Subscripts

aw	= adiabatic wall
lam	= laminar
O_2	= oxygen
ref	= reference
t	= stagnation
turb	= turbulent
tran	= transient

* Head, Aero-Thermodynamics Lab., Aerodynamics Div., National Aerospace Laboratory, 7-44-1 Jindaiji-Higashi, Chofu, Tokyo 182-8522, Japan (e-mail: asai@nal.go.jp)
† Head and Professor, School of Aeronautics and Astronautics, Purdue University, 1282 Grissom Hall, West Lafayette, IN 47907, USA (e-mail: sulivan@ecn.purdue.edu)

INTRODUCTION

One of the major advances made in modern wind tunnel testing is the cryogenic wind tunnel technology developed at NASA Langley Research Center [1]. A cryogenic wind tunnel provides a realistic means of simulating high Reynolds number flow. Cooling the test gas to near the liquid nitrogen (LN_2) temperature increases Reynolds number by more than a factor of 7. A large-scale pressurized cryogenic wind tunnel such as the National Transonic Facility (NTF) at NASA Langley and the European Transonic Wind Tunnel (ETW) can achieve full-scale flight Reynolds number at transonic speeds with subscale transport models.

In these cryogenic wind tunnels, the ability to measure temperature distribution on the model surface is the most critical testing requirement because it is related to the boundary-layer transition from laminar to turbulent flows. For this purpose, a standard infrared(IR) camera is often used in conventional ambient-temperature wind tunnels. However, this type of IR camera is not suitable for use at cryogenic temperatures because the overall level of IR radiation rapidly decreases with decreasing temperature and the peak of the radiated energy is shifted to longer wavelengths [2]. A special long-wave IR camera cooled by liquid helium has to be used to detect a small temperature difference caused by boundary-layer transition [3].

Measurement of surface pressure distribution is also an important issue in cryogenic wind tunnel testing. At present, the most common practice is to use pressure taps and electric pressure scanners. Pressure scanners are usually housed inside the model and maintained at ambient temperature using an electric heater. It was pointed out, however, that heat transfer through the model substrate could affect boundary layer evolution on the external surface (non-adiabatic wall effects). Also, a care must be taken in sizing pressure taps to prevent premature transition of boundary layer.

In this paper, we present a new technology for global surface temperature and pressure measurements in a cryogenic wind tunnel. This technology uses luminescent molecules as temperature and pressure sensors. Since the late 1980's, temperature-sensitive paint (TSP) and pressure-sensitive paint (PSP) have been widely used in ambient-temperature wind tunnel tests [4], [5]. These paints incorporate luminescent molecules in a paint, which can be applied to any aerodynamic model surface. Through the photo-physical phenomena known as thermal- and oxygen quenching, the luminescence intensity of the paint emission is related to temperature and/or pressure. Hence, from the detected luminescent intensity, temperature and pressure distributions over the model surfaces can be determined.

The purpose of the present study is develop the luminescent paint technology that allows one to measure surface temperature and pressure in the adverse flow condition in a cryogenic wind tunnel. Various chemicals has been synthesized and tested using a cryogenic calibration device. Also, a new application technique based on anodic porous alumina has been developed for a PSP. Described in this paper are the fundamentals of TSP and PSP, their formulations and luminescent characteristics, data reduction, and calibration procedures. Experimental results from the tests conducted in the 0.1-m Transonic Cryogenic Wind Tunnel at the National Aerospace Laboratory are also presented. From our experiences, the status and the prospect on applications of the luminescent paint technology to cryogenic wind tunnel testing is discussed.

FUNDAMENTALS

Figure 1 is a schematic showing a luminescent paint system. Light to excite the luminescence molecules in the paint is directed at the model surface and luminescent light is emitted by the molecules.

The quantum efficiency of luminescent paint , Φ, can be expressed as follows;

$$\Phi = \frac{I}{I_a} = \frac{k_L}{k_L + k_D + k_Q[O_2]} \tag{1}$$

where k_L is the rate constant for luminescence emission, k_D is the rate constant for radiationless deactivation, k_Q is the rate constant for oxygen quenching, and [O2] is the concentration of oxygen.

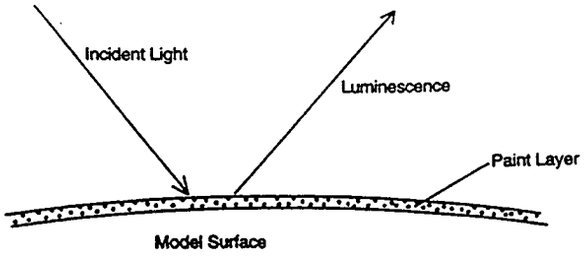

Fig. 1: Schematic of a TSP/PSP layer

Dividing eq. (1) into the quantum efficiency in the absence of oxygen, i.e., $k_L/(K_D+k_Q)$, one can obtain the Stern-Volmer equation.

$$\frac{I_o}{I}\left(=\frac{\Phi_o}{\Phi}\right) = 1 + K_q[O_2] \tag{2}$$

where I is the luminescence intensity, Io is its maximum value in the absence of oxygen, and Kq is the Stern-Volmer quenching constant.

For most paints, $[O_2]$ is proportional to PO2 (Henry's law). If the mole fraction of oxygen in the working gas is constant (0.21 for air), P_{O2} is proportional to local static pressure, P. Using these relations, eq. (2) can be rewritten in terms of local static pressure.

$$\frac{I_o}{I} = 1 + Kp_{o2} = 1 + K\bar{X}_{o2}p \tag{3}$$

where K is the quenching constant with respect to P_{O2} and $\bar{X}_{o2}$ is the mole fraction of oxygen in the working gas.

By taking the ratio between I and a reference intensity Iref at a known constant reference pressure Pref, the Stern-Volmer relation can be expressed as;

$$\frac{I_{ref}}{I} = A(T) + B(T)\frac{p}{p_{ref}} \tag{4}$$

where A and B are calibration constants of the paint which have to be determined by experiments. This equation gives a basis for pressure measurement by PSP.

For a TSP, it is assumed that the luminescent molecules are not quenched by oxygen (kQ=0) or the paint layer is not oxygen permeable ([O2]=0). Hence, the calibration relation becomes much simpler. For practical applications, the relation between the luminescent intensity and temperature can be expressed in a functional form

$$\frac{I(T)}{I(T_{ref})} = f(T/T_{ref}) \tag{5}$$

where Tref is the reference temperature. This empirical expression can be fitted to a polynomial equation over a certain temperature range.

BOUNDARY-LAYER TRANSITION DETECTION BY TEMPERATURE SENSITIVE LUMINESCENT PAINT

TSP Formulation [6],[7],[8]

Temperature sensitive paint for use in a cryogenic wind tunnel should have two specific characteristics: (1) high temperature sensitivity over the operating range of a cryogenic wind tunnel and (2) robust attachment to model surface at cryogenic temperature. The development of such paints has been pioneered by Purdue University in USA. Campbell, et al. [6], [7] calibrated a large number of

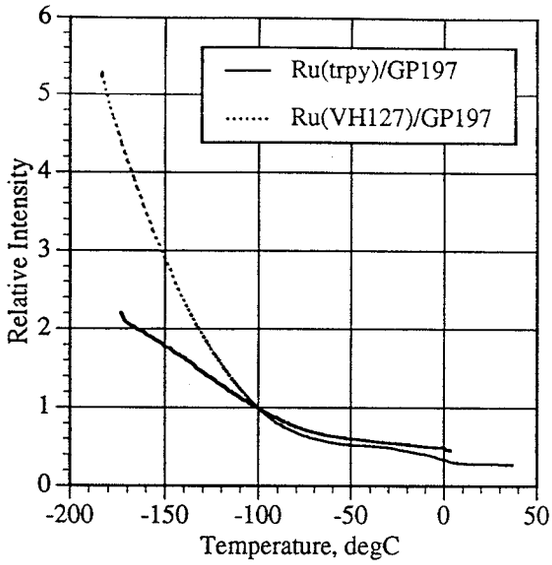

Fig. 2: Calibration curves for TSPs, Ru(trpy), and Ru(VH127) in GP197

compounds in various polymer bases and found that the luminescence of ruthenium-base paints was strongly sensitive to temperature over the cryogenic temperature range. Following are some successful cryogenic TSP formulations [5], [7].

1) Ru(trpy) in GP197
2) Ru(VH127) in GP197
3) Ru(trpy)(phtrpy) in GP197
4) Ru(trpy) in Chroma Clear, etc.

GP197 is a dimethylsiloxane polymer commercially available (Genesse Polymers Corp.) Chroma Clear is polyurethane-based polymer produced by Du Pont. Ru(trpy), Ru(VH127), and Ru(trpy)(phtrpy) are ruthenium complexes synthesized in a laboratory. These paints can be sprayed onto model surfaces using an airbrush. After being dried for hours, the painted surface can be polished to desired smoothness.

Figure 2 shows luminescence intensity as a function of temperature for Ru(trpy) and Ru(VH127) paints. As shown, both paints have a strong temperature dependence over the range from 90 to 220K. The maximum logarithmic slope, $\Delta \ln(I/I_{ref})/\Delta T$, is about -1.3% and -2.2% per degree for Ru(trpy) and Ru(VH127) respectively. Luminescence intensity decreases with increasing temperature. This is resulting from that non-radiative deactivation begins to dominate radiative transitions as temperature increases

Application of the paint on a model surface is another concern. The paint must adhere to the surface strongly enough to withstand the flow. Also, the difference in thermal contraction between the paint and model must not create any cracks which may trigger premature transition. We found that the paint thickness was critical to prevent the coating from cracking or rippling. When the thickness is less than a certain critical value (say 10 microns), the coating keeps smooth even at cryogenic temperatures.

Description of Experiment [9]

Two formulations, Ru(trpy)-GP197 and Ru(VH127)-GP197 have been used to detect transition on airfoil models in the 0.1-m Transonic Cryogenic Wind Tunnel at NAL (Fig.3). This tunnel is a closed-circuit, fan-driven wind tunnel operated with cryogenic nitrogen as the working gas. The test section is 0.1m square and equipped with slotted top and bottom walls and solid side walls [10].

The cross section of the model is a symmetrical NACA 64A012 laminar airfoil. The chord length is 0.05m and the span is 0.1m. They are made of white glass ceramic (MACOR) and stainless steel. The stainless steel model is covered with a 50-micron thick white Mylar insulating layer or polyurethane-based white paint to increase surface temperature variation.

Proper thickness of the insulating layers can be estimated by a simple thermal analysis based on one-dimensional heat transfer in thin insulating layer [9]. A thicker coating provides good thermal insulation while a thinner coating is desirable for strong attachment. The suitable insulation thickness has to be determined by a tradeoff between these conflicting requirements.

Figure 4 shows a schematic of optical setup for this experiment. An excitation light source is a 300W Xenon lump with a band pass filter (475±50nm), and a collimating lens. A dichroic mirror is used to separate paint emission from excitation light. The emission from the

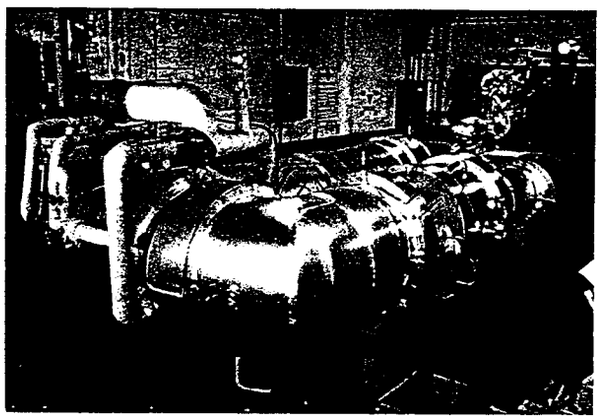

Fig. 3: NAL 0.1-m Transonic Cryogenic Wind Tunnel

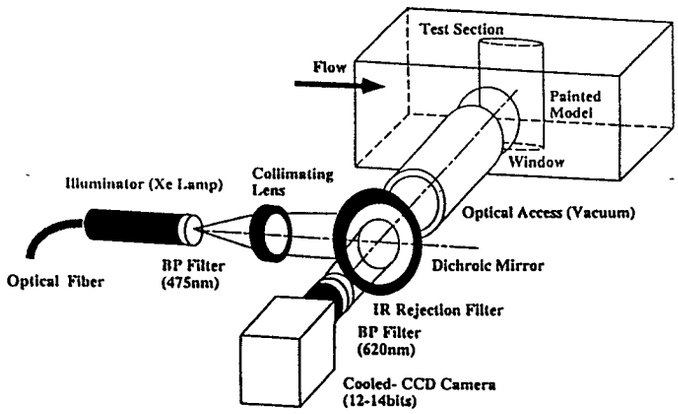

Fig. 4: Schematic of optical setup in the 0.1-m TCWT paint is detected with a digital camera with a cooled CCD.

This camera has a 12-bit gray-scale resolution and 1000x1018 pixel spatial resolution. A band pass filter (620±20nm) is placed over the camera lens.

Test Procedure and Data Reduction

The adiabatic wall temperature difference, ΔT_{aw}, across transition line can be evaluated from the following simple relationship.

$$\Delta T_{aw} = \left(\frac{M^2}{5+M^2}\right)\Delta r \cdot T_t \text{ where } \Delta r = r_{turb} - r_{lam} \qquad (6)$$

The recovery factor values, r, are 0.84 and 0.896 for laminar and turbulent flows. The temperature difference across transition line is less than 1 degree at cryogenic free-stream temperatures. In reality, it is difficult to resolve such a small temperature difference even using a high-resolution camera.

To enhance the temperature difference across the transition line, both (1) a transient method of rapidly changing the free-stream temperature and (2) a steady heating method were employed (Fig.5). The cryogenic wind tunnel is cooled by continuous LN_2 injection and a jump of the flow temperature can be easily induced by a rapid change in LN_2 flow rate. For a steady heating, a thin film resistance heater was installed inside the stainless steel model to heat the model substrate uniformly. Since convective heat transfer coefficient in turbulent flow is much higher than in laminar flow, temperature difference caused by the transition can be augmented by either transient and steady methods.

Figure 6 shows the image processing sequence for transition detection. Figure 6(a) is a luminescent intensity image taken at steady state condition while Fig. 6(b) is taken during cooling process. The transient image (Fig.6 (b)) is a little bit brighter than the steady-state image (Fig.6 (a)) since the former was taken during cooling process. Transition signatures are not evident in these raw images due to uneven coating thickness and non-uniform illumination.

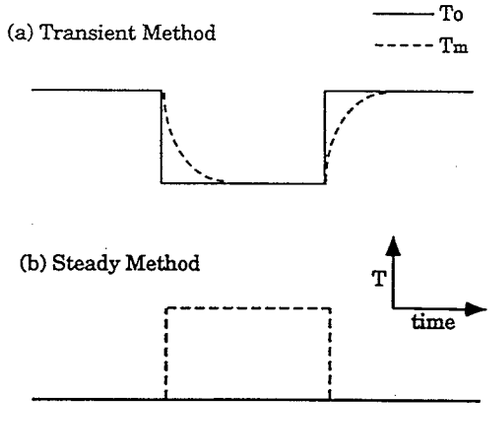

Fig. 5: Procedures of thermal signature enhancement techniques

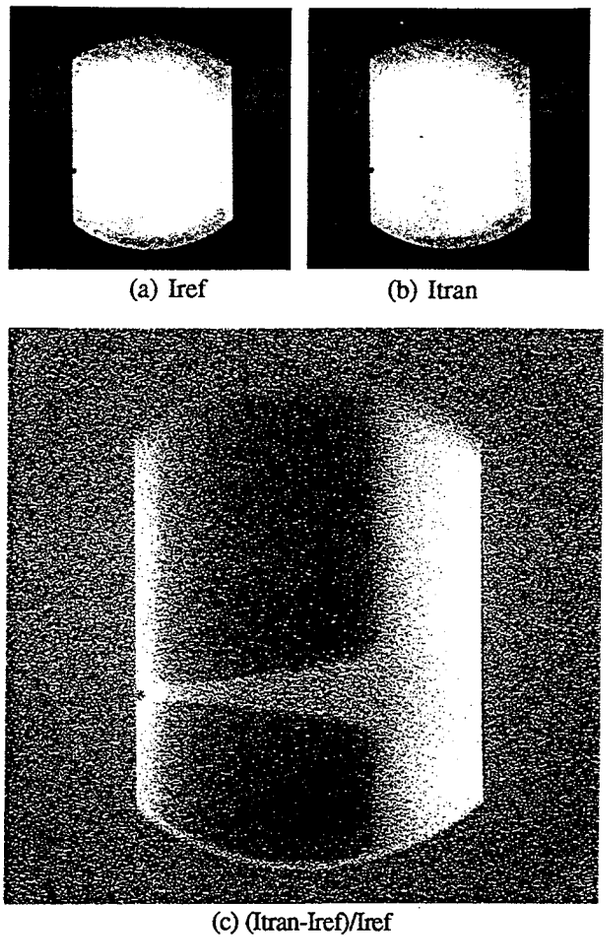

(a) Iref (b) Itran

(c) (Itran-Iref)/Iref

Fig. 6: Image processing sequence for transition detection, M=0.4, Tt=150K, ΔT= -7.5K

Figure 6(c) is a processed image obtained by subtracting image (b) from image (a) and then by normalizing it with the steady-state image. The natural transition line is clearly identified as an edge of the brightness. The turbulent wedge induced by the leading-edge roughness is clearly visible as well. Turbulent region appears bright because it is cooled faster due to higher heat transfer. Obviously, the ratioing process has eliminated the effects of uneven paint layer and non-uniform excitation.

Figure 7 shows chordwise luminescence intensity profiles extracted from Fig. 6(c) at two spanwise locations. One is through natural transition region and other is through forced transition region. The plot clearly illustrates the evolution of the boundary layer from laminar to turbulent flows. The high intensity region near the leading edge is caused by high local heat transfer in thin laminar boundary layer. The intensity jump at about x/c=66% signifies the position of transition onset. Transition to turbulence is completed at about x/c=79%.

The transition image becomes much clearer with increasing temperature jump. This is the case for a steady heating method too. One of the reasons for this contrast is that the spatial temperature gradient across the transition line increases with increasing ΔT. However, ΔT must be kept as small as possible to avoid the undesirable effect of non-adiabatic wall. We can check this by comparing several images taken for different temperature steps. In the

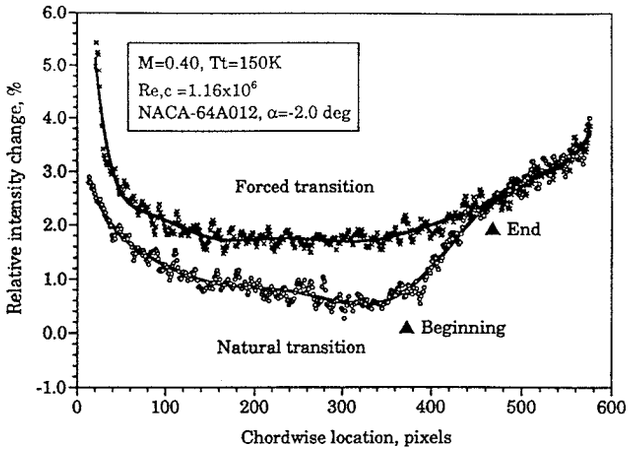

Fig. 7: Chordwise Luminescent intensity profiles through forced and natural transition regions

present experiment, the transition line can be identified even at $\Delta T/T_t = 1\%$.

Reynolds Number Effects

Figures 8 show the transition images taken at various Reynolds numbers. Figures 8(a) through (c) show the images taken at a constant temperature(140 K) and at stagnation pressures from 110 to 180 kPa. On the other hand, Figs. 8(a), (d), (e), and (f) represent the images at various stagnation temperatures from 140K to 100K when the tunnel stagnation pressure is constant (110kPa). It is noted that Reynolds number in Figs. 8(b) and (c) are the same as that in Figs. 8(c) and (f).

As shown in these figures, the number of turbulent wedges increases with increasing Reynolds number while the location of natural transition line appears unchanged with Reynolds number. The similar change in transition pattern can be observed through either way of adjusting Reynolds number. The turbulent wedges at higher Reynolds numbers are possibly caused by small imperfections near the leading edge having a size close to the critical roughness height.

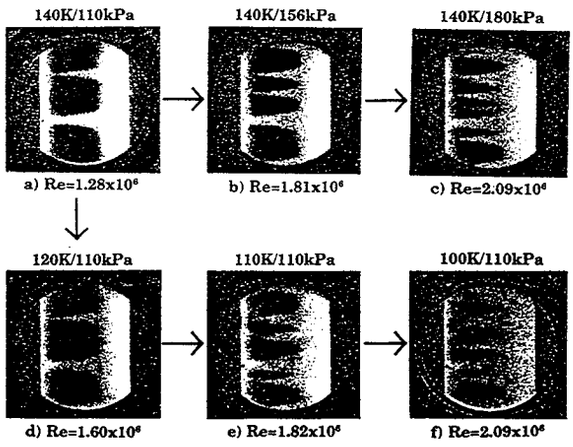

Fig. 8: Transition images obtained for varying Reynolds numbers

Figure 9 is the transition image taken at 90K and 190kPa. Reynolds number based on the chord length is 4.24 million. This image was obtained using the steady heating method because transient cooling would cause liquefaction of the working gas. It is seen that most of the boundary layers are prematurely tripped at the leading edge. Some defects near the leading edge may be attributed to contamination of the paint layer. Since at cryogenic condition the boundary layer on the model is extremely thin due to high unit Reynolds number and small-scale models, even very small cracks may trip the boundary layer. A special care must be taken for the surface roughness of the painted surfaces.

Images Taken at Transonic Speeds

Figure 10 shows a transition image taken at Mach number=0.81 and at $\alpha=+2^{\circ}$. The steady heating method was used again to avoid producing undesirable disturbances in free stream. An interesting feature shown in these images is that, besides the transition lines and the turbulent

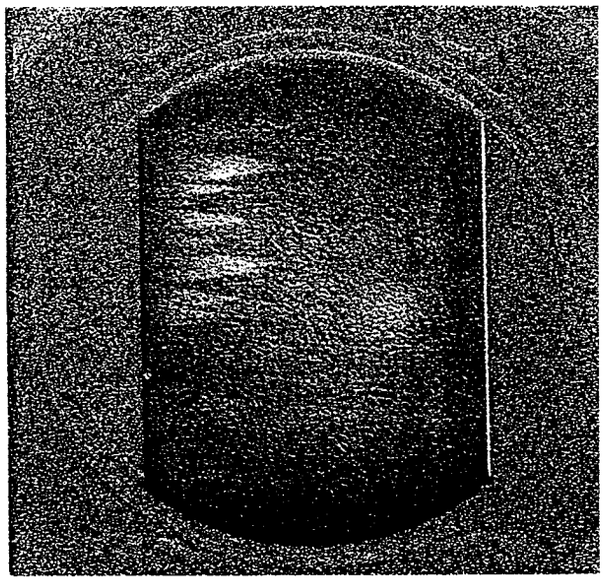

Fig. 9: Transition image taken at Tt=90K and Pt=190K

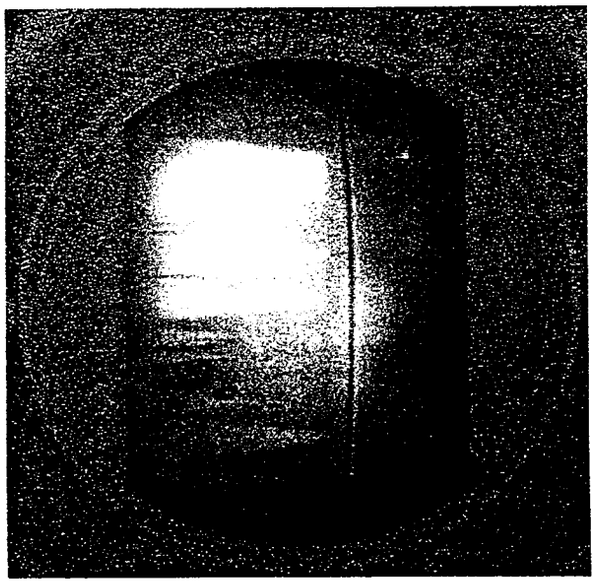

Fig. 10: Image obtained at M=0.81, Tt=120K

wedges, a shock wave spanning the model is clearly observed in the same image. This is a well-known image of a shock wave in shadowgraph. Note that we used a near parallel beam of light to excite the luminescent paint. The model surface actually acted as an efficient screen for shadow projection. The shadow of a shock wave is relating to a change in the second derivative of the refractive index (or density) in a shock wave, thus appears as the dark and bright contour. These figures illustrate the usefulness of the paint technique to capture the details of the flow field, including boundary-layer transition and shock waves.

SURFACE PRESSURE MEASUREMENT BY PRESSURE-SENSITIVE LUMINESCENT COATING

New PSP Coating Technology [11], [12], [13]

In nature, pressure-sensitive paints are more complicated and difficult to be implemented than temperature-sensitive paints. PSPs utilize the sensitivity of luminescent molecules to the presence of molecular oxygen. An inherent problem arises here since the working gas in a cryogenic wind tunnel is practically pure nitrogen. We need oxygen but injecting a large amount of oxygen into the tunnel is not permitted from the viewpoints of safety and cost. In addition, polymer matrices which are commonly used as the binder become non-permeable to gas below a certain temperature [13].

To alleviate this adverse effect of low temperature on polymer binders, a new coating technology has been developed [11]. Figure 11 is a schematic comparing our new coating to conventional polymer-based coatings. In the conventional method, luminescent molecules are distributed in a polymer matrix. On the other hand, in the present method, luminescent molecules are deposited directly on the model surfaces. It is well known that porous alumina is formed on aluminum or aluminum alloy by anodizing in sulfuric or oxalic solution. As in seen in Scanning Electron Microscopy (SEM) image in Fig.12, thousands of micropores of about 30 nm are uniformly distributed over the surface of an anodized layer. We can incorporate probe molecules such as our ruthenium-based sensor in these micropores by an electrochemical deposition process.

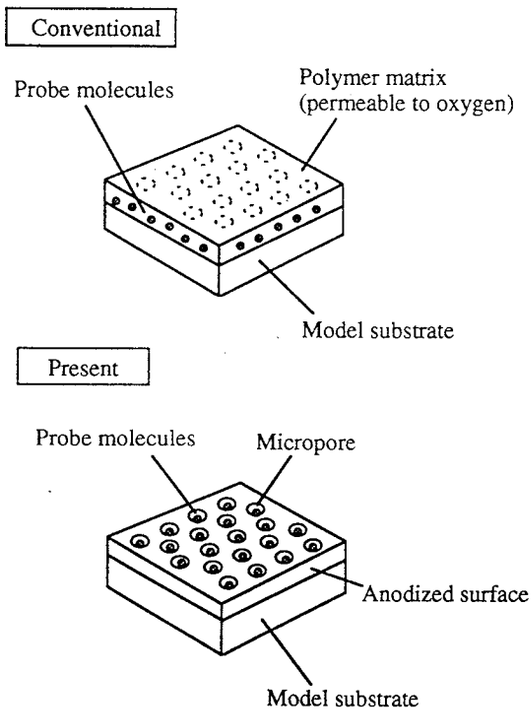

Fig. 11: Schematic comparing polymer-based coating and coating based on anodized surface.

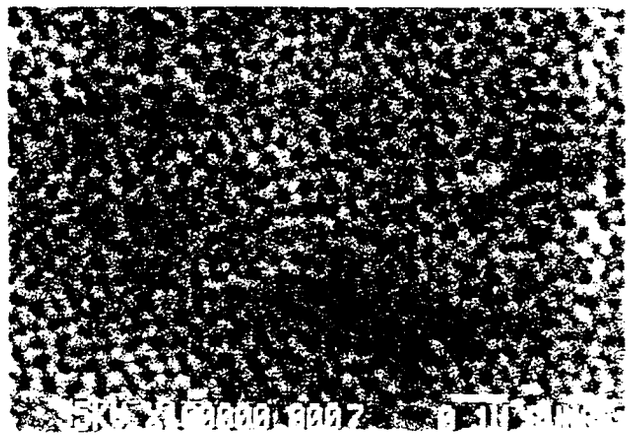

Fig. 12: SEM image of anodized porous alumina

A calibration curve for a coating based on this anodized surface is shown is Fig.13. It is interesting to note that the coating's sensitivity to oxygen varies dramatically with oxygen concentration. The sensitivity, $(\Delta I/Io)/\Delta O_2[\%]$ is as high as 40 at near zero-oxygen condition. This large quenching constant (K) allows us to measure pressure in the nitrogen-based working gas of a cryogenic wind tunnel which has very low oxygen mole fraction ($\bar{X}_{o_2}$) .

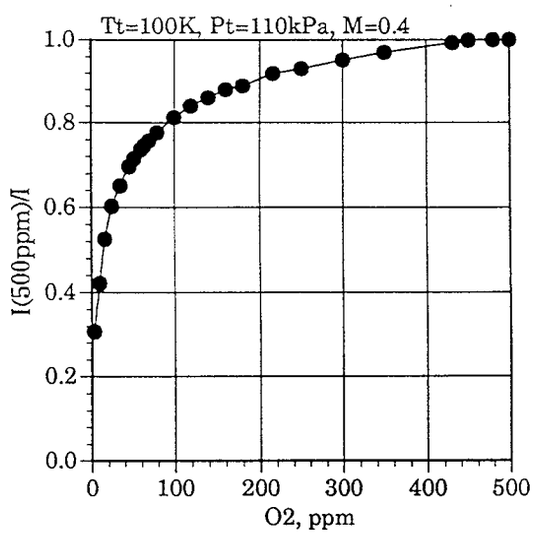

Fig. 13: Calibration curves for coating based on anodized surface at cryogenic temperatures (T=100K)

Description of Experiment

To demonstrate the capability of the new coating based on anodic porous alumina, a 14-% thick circular-arc bump model was tested in the NAL 0.1-m TCWT. This model is equipped with 16 pressure taps in the centerline and two removable strip parts in two spanwise locations (Fig.14) . A luminescent coating was applied on a strip part made of aluminum. We used the same measurement system as used in transition tests. The coating was excited by a Xenon light with a blue filter (475±50nm) and the luminescence image was acquired using a digital camera with an IR rejection filter and a red high pass filer (600nm or higher).

Figure 15 is a schematic diagram of experimental setup. Oxygen gas was injected through a strut located just downstream of the test section. A small amount of the exhaust gas was sampled and fed into a Zirconia (ZrO2) oxygen sensor to monitor the oxygen mole fraction in the flow, $\overline{X}_{o_2}$. The ZrO2 sensor was calibrated prior to each run using a standard gas with known oxygen concentration. In the present experiments, $\overline{X}_{o_2}$ was varied from near zero (no oxygen injection) to 500ppm. Mach number was

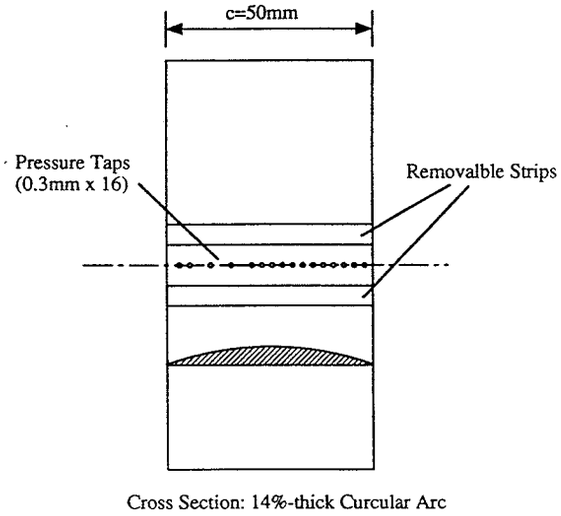

Fig. 14: 14%-thick circular-arc bump model .

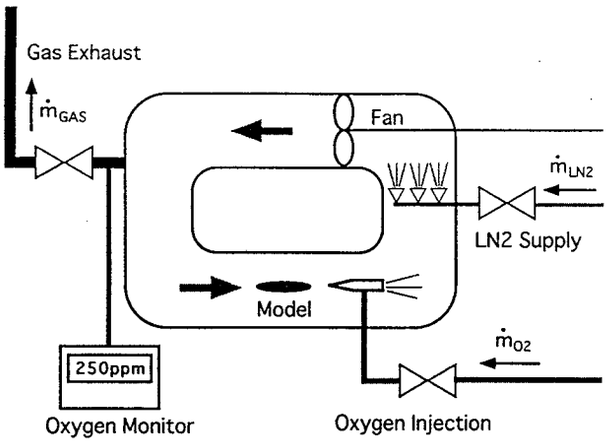

Fig. 15: Schematic diagram of experimental setup for PSP tests in a cryogenic wind tunnel.

varied from 0.4 to 0.84, while stagnation temperature and stagnation pressure were kept constant at 100 Kelvin and 110 kPa respectively.

Data Reduction

Any pressure-sensitive coating has the effects of spatial non-uniformity in excitation light and coating thickness. These undesirable effects should be cancelled out by taking the ratio of luminescence intensity, I, with respect to the intensity at a reference condition, I_{ref}, as long as the intensity-based technique is employed.

We have two choices for the reference condition. One obvious choice is to use an image taken at the zero-quenching condition, since the working gas in a cryogenic wind tunnel is basically nitrogen. Ideally, the gas in a cryogenic wind tunnel with no oxygen injection is pure nitrogen. But, in reality, some amount of oxygen exists in the test gas even when no oxygen is injected. This residual oxygen (order of 10 ppm) is believed to have come from the liquid nitrogen. Due to extremely high sensitivity to oxygen of the anodic coating, the pressure field on the model induces a variation of luminescence intensity in the presence of the residual oxygen. The intensity for a no-injection case can never be a constant. As a result, a direct application of the basic Stern-Volmer relationship (eq.(3)) fails in real situations.

The second choice for the reference image is to use an image taken with no wind as the reference. In a cryogenic wind tunnel, however, a wind-off still condition cannot be attained because the tunnel condition is maintained by a continuous injection of liquid nitrogen. The practical alternative is to use the image taken at low speeds, say M=0.05, where the dynamic pressure is so small that we can assume the reference pressure is uniform over the whole surface at a known constant value. By ratioing the wind-on image and the low-speed reference image, we can get eq. (4). The coefficients A and B are coating sensitivity coefficients that should be determined by experimental calibration.

Figure 16 shows the luminescence intensity profiles at two different Mach numbers, M=0.4 and M=0.82. The intensity in the center of coating strips (20 pixels in the spanwise direction) are averaged. Both data were taken at the same temperature (Tt=100 K) and oxygen mole fraction ($\overline{X}_{o_2}$=250ppm). Note that the difference between the two intensities is only about 5% of the reference value.

We use the image at M=0.4 as a reference image because 0.4 is the lowest Mach number attainable in the NAL 0.1-m TCWT. This is not the case for larger cryogenic wind tunnels which allow operation at lower speeds. Figure 17 is a plot of the ratio of the high-speed intensity with the low-speed reference intensity. It is evident that the intensity ratio is representing a chordwise variation in surface pressure. Flow accelerates from the leading edge to the maximum-thickness position and causes an abrupt pressure jump due to shock at about x/c=0.7. A pair of intensity spikes observed at the foot of a shock is the shadowgraph image of the shock.

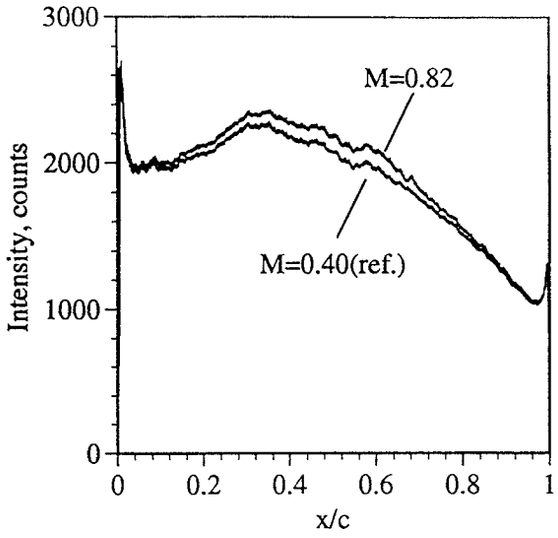

Fig. 16: Luminescence intensity profiles at M=0.82 and M=0.4(reference) ; Tt=100K and [O2]=250ppm.

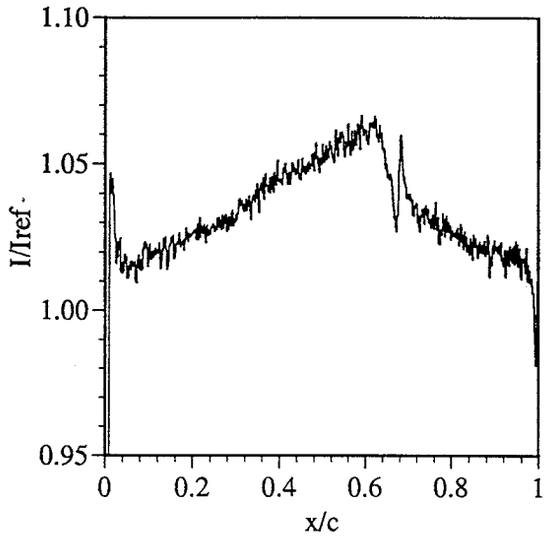

Fig. 17: Luminescence intensity ratio; intensity data taken at low speeds (M=0.4) being used as a reference.

Calibration of PSP

To calculate pressure from the measured intensity ratio, the coefficients, A and B, in eq. (5) have to be determined by experimental calibration of the PSP coating. There are two calibration approaches, *in situ* and *a priori*, which have been widely employed to determine the paint sensitivity coefficients.

The *in situ* method is performed on a model equipped with pressure taps during the run condition, using data from pressure taps and the PSP at spatially corresponding locations. On the other hand, the *a priori* method involves the calibration of the PSP coating under static conditions. This usually takes place in a pressure- and temperature-controlled chamber on a test coupon coated with the same batch of the paint applied on the model (*a priori* coupon calibration). One attractive alternative to the coupon test is to determine the calibration constants in a wind tunnel by varying the oxygen concentration at low speed and taking images of the model coated with PSP (*a priori* wind tunnel calibration). This allows pixel by pixel calibration of the PSP coating.

Figure 18 is a plot of Iref/I versus pressure tap measurements (*in situ* calibration). As is evident, the relationship between Iref/I and P/Pref is linear. Also noted is that the data obtained upstream and downstream a shock wave are fit on a single line. In a cryogenic wind tunnel, a variation in surface temperature is so small that we can assume the model surface is fairly isothermal . Hence, we can neglect temperature dependence of the PSP coating and use a single calibration curve for the entire surface of the model.

Figure 19 compares PSP data converted from Iref/I using the calibration curve in Fig. 18 with tap measurements. Except near the leading edge and the trailing edge where the S/N ratio is poor, the paint-derived data are in good agreement with the tap measurements. Figures 20 (a) through (d) show Cp distributions derived from the measured intensity distributions for M=0.75 to 0.84. The paint-derived data are well representing a variation of pressure distribution with an increase of Mach number. It is seen that the PSP coating could clearly identify shock wave strength and locations, and flow separation induced by a shock.

One of the problems we found in the present experiment is the unevenness of oxygen sensitivity over the coating surface. The paint sensitivity was not uniform along the chord. Our recent experiment suggests that the oxygen sensitivity is dependent on the thickness of anodized layer and a way of depositing luminescent molecules. We need to improve the uniformity of the PSP coating to employ the *in situ* calibration for more complicated 3-D configurations.

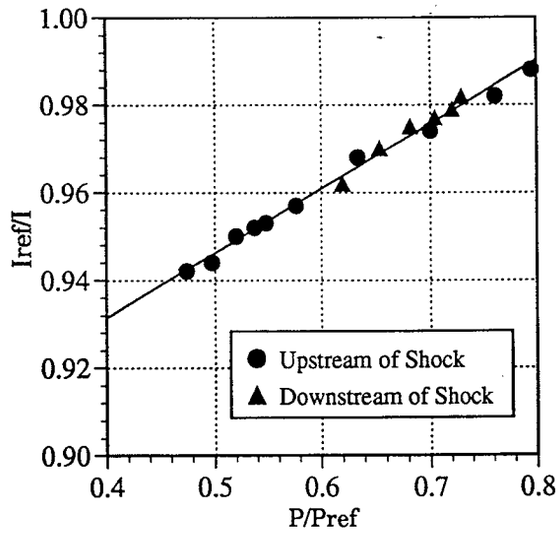

Fig. 18: *In situ* calibration; curve fit of luminescence intensity data and pressure tap data; M=0.82, Tt=100K, [O2]=250ppm.

Ideally, the *a priori* calibration is desirable because no pressure tap measurements are required. At present stage, however, the *in situ* calibration is the only operational method. We found there was a significant difference between *a priori* and *in situ* calibrations. It is considered that this difference is related to the accuracy of oxygen concentration measurement. An O2 measurement of the ZrO2 sensor used in this study is repeatable but its accuracy in this low oxygen concentration range is not known. Likewise, the standard gas used in coupon calibration also has some uncertainty in the oxygen level. A careful calibration will be required to attain absolute accuracy in oxygen measurement. If we could measure the oxygen mole fraction in the gas with a sufficiently high accuracy, the *a priori* approach would work as expected.

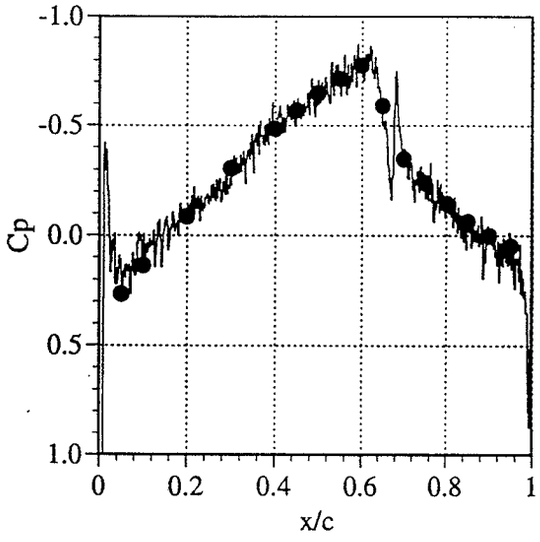

Fig. 19: Comparison of chordwise pressure distributions obtained from PSP coating and pressure taps (●).

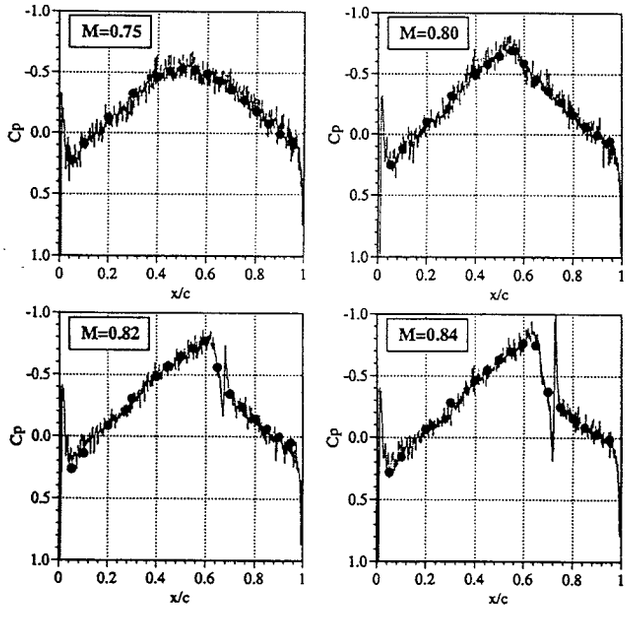

Fig. 20: Comparison of luminescent paint coating and pressure tap data at M=0.75 to 0.84

CONCLUDING REMARKS

The cryogenic temperature-sensitive paint technique has been developed and established. Using the TSPs composed of ruthenium complex and silicone polymer, boundary-layer transitions can be clearly visualized on airfoil models over a cryogenic temperature range form 90-150 Kelvin. Thermal signatures due to transition can be enhanced just by introducing a step change in the injection rate of liquid nitrogen. The shadow of shock waves can be also visualized using the luminescent paint technique.

A new luminescent coating using anodic porous alumina has been developed. This coating has an extremely high oxygen sensitivity at low oxygen concentration. Unlike the conventional polymer-based coating, this coating maintains its sensitivity to oxygen even at cryogenic temperatures. Using the low-speed data as a reference, the pressure jump due to a shock wave and resulting flow separation was clearly identified at transonic Mach numbers. The *in situ* calibration works in cryogenic wind tunnel testing. The isothermal assumption is valid and the effect of temperature dependence of the PSP coating can be ignored in a cryogenic wind tunnel.

The anodized PSP coating has been proved to work, but it is still in the developing stage. There are some problems associated with paint uniformity, stability (aging), and measurement accuracy. It is also found the quenching process to be moisture dependent. We have to solve these problems before using this technology in practical testing. A fundamental study by chemists and material scientists will be needed to improve coating characteristics.

As has demonstrated in the present study, luminescent paints works in the adverse flow condition in a cryogenic wind tunnel. According to the basic photo-physical theory, the luminescence is the strongest at low temperature and at low oxygen concentration. This suggests that the cryogenic luminescent paint technology that is superior to that for ambient temperature testing could be developed.

ACKNOWLEDGMENTS

This work is a team effort which includes the participants from NAL in Japan and Purdue University in the USA. First of all, the authors would like to acknowledge Tianshu Liu of High Tech Corporation and Brian Campbell of Aerojet for informative discussions and their contributions to PSP and TSP development. We would like to thank Hiroshi Kanda, Tetsuya Kunimasu, and Yoshimi Iijima of NAL for their contribution in the tests in the NAL 0.1-m TCWT. We would also like to acknowledge Corey Cunningham and Rick Erausquin at Purdue University for their efforts on paint development and calibration. Lastly, we thank Hirotaka Sakaue at Purdue for preparing some of the PSP samples and for providing a SEM image.

REFERENCE

1. Goodyer, M. J. and Kilgore, R. A., "The High Reynolds Number Cryogenic Wind Tunnel", *AIAA Journal*, Vol. 11, No. 5, May 1973, pp. 613-619.

2. Gartenberg, E. and Wright, R. E., "Boundary-Layer Transition Detection with Infrared Imaging Emphasizing Cryogenic Applications", *AIAA Journal*, Vol. 32, No. 9, Sep. 1994, pp. 1875-1882.

3. Anon, "Infrared cameras for transition detection", ETW News, Issue No.1 , May 1994.

4. McLachlan, B. G. and Bell, J. H., "Pressure-Sensitive Paint in Aerodynamic Testing", *Experimental Thermal and Fluid Science* , Vol. 10, 1995, pp. 470-485.

5 Liu, T., Campbell, B. T., Burns, S. P., and Sullivan, J. P., "Temperature- and Pressure-Sensitive Luminescent Paints in Aerodynamics", *Applied Mechanics Reviews*, vol. 50, no.4, pp.227-246, April 1997

6. Campbell, B. T., Liu, T., and Sullivan, J. P., "Temperature Measurement Using Fluorescent Molecules", *6th International Symposium on Application of Laser Techniques to Fluid Mechanics*, Lisbon, Portugal, July 20-23, 1992.

7. Campbell, B. T., "Temperature Sensitive Fluorescent Paints for Aerodynamic Applications", M.S. Thesis, School of Aeronautics and Astronautics, Purdue University, West Lafayette, IN, May 1993.

8. Campbell, B. T., Liu, T., and Sullivan, J. P., "Temperature Sensitive Fluorescent Paint Systems", AIAA Paper 94-2483, June 1994.

9. Asai, K., Kanda, H., Kunimasu, T., Liu, T. and Sullivan, J. P., "Boundary-Layer Transition Detection in a Cryogenic Wind Tunnel Using Luminescence Paint", *J. of Aircraft*, Vol. 34. No.1, Jan.-Feb. 1997, see also AIAA Paper 96-2185.

10. Sawada, H. and Aoki, T., "NAL 10cm Cryogenic Wind Tunnel", *Proc. of PICAST '1 Vol. III*, Taiwan, Dec. 1993, pp.1143-1150.

11. Asai, K., "Luminescent Coating with an Extremely High Oxygen Sensitivity at Low Temperatures", Patent Pending H9-207351, July 1997, Japan.

12. Asai, K., Kanda, H., Cunningham, C.T., Erausquin, R.G., and Sullivan, J. P., "Surface Pressure Measurement in a Cryogenic Wind Tunnel By Using Luminescent Coating", Proc. of the 13th ICIASF, Montrey CA, USA, Sept.-Oct. 1997.

13. Erausquin, R.G., Cunningham, C.T., Sullivan, J. P., Asai, K., Kanda, H., Kunimasu, T., and Y. Iijima, "Cryogenic Pressure Sensitive Fluorescent Paint Systems", AIAA Paper 98-0588, Jan. 1998.